Very Large Telescope Interferometer observations of the dust geometry around R Coronae Borealis stars

S.N. Bright, O. Chesneau, G.C. Clayton, O. de Marco, I.C. Leão, J. Nordhaus, J.S. Gallagher

Monthly Notices
of the
ROYAL ASTRONOMICAL SOCIETY

Mon. Not. R. Astron. Soc. **414,** 1195–1206 (2011) doi:10.1111/j.1365-2966.2011.18449.x

Very Large Telescope Interferometer observations of the dust geometry around R Coronae Borealis stars⋆

S. N. Bright,[1]† O. Chesneau,[2] G. C. Clayton,[3] O. De Marco,[1] I. C. Leão,[4] J. Nordhaus[5] and J. S. Gallagher[3]

[1]*Department of Physics and Astronomy, Macquarie University, Sydney, NSW 2109, Australia*
[2]*UMR 6525 H. Fizeau, Univ. Nice Sophia Antipolis, CNRS, Observatoire de la Côte d'Azur, Av. Copernic, F-06130 Grasse, France*
[3]*Department of Physics and Astronomy, Louisiana State University, Baton Rouge, LA 70803, USA*
[4]*Departamento de Física, Universidade Federal do Rio Grande do Norte, 59072-970 Natal, RN, Brazil*
[5]*Department of Astrophysical Sciences, Princeton University, Princeton, NJ 08544, USA*

Accepted 2011 January 31. Received 2011 January 27; in original form 2010 September 22

ABSTRACT

We are investigating the formation and evolution of dust around the hydrogen-deficient supergiants known as R Coronae Borealis (RCB) stars. We aim to determine the connection between the probable merger past of these stars and their current dust-production activities.

We carried out high angular resolution interferometric observations of three RCB stars, namely RY Sgr, V CrA and V854 Cen, with the mid-infrared interferometer (MIDI) on the Very Large Telescope Interferometer (VLTI), using two telescope pairs. The baselines ranged from 30 to 60 m, allowing us to probe the dusty environment at very small spatial scales (∼50 mas or $400R_\star$). The observations of the RCB star dust environments were interpreted using both geometrical models and one-dimensional radiative transfer codes.

From our analysis, we find that asymmetric circumstellar material is apparent in RY Sgr, may also exist in V CrA and is possible for V854 Cen. Overall, we find that our observations are consistent with dust forming in clumps ejected randomly around the RCB star so that over time they create a spherically symmetric distribution of dust. However, we conclude that the determination of whether there is a preferred plane of dust ejection must wait until a time series of observations are obtained.

Key words: techniques: high angular resolution – techniques: interferometric – stars: individual: RY Sgr – stars: individual: V CrA – stars: individual: V854 Cen – stars: mass-loss.

1 INTRODUCTION

The R Coronae Borealis (RCB) stars are a small group of carbon-rich supergiants. Their defining characteristics are hydrogen deficiency and unusual variability (Clayton 1996). RCB stars undergo massive declines of up to 8 mag due to the formation of carbon dust at irregular intervals. Two scenarios (Iben Tutukov & Yungelson 1996; Saio & Jeffery 2002) have been proposed for the origin of RCB stars: the first is the merger of helium and carbon–oxygen white dwarfs that temporarily results in a swollen star (Webbink 1984), while the second is a final helium-shell flash taking place on a white dwarf that temporarily increases the star's radius to supergiant dimensions (Fujimoto 1977; Renzini 1979). Final-flash stars have been directly observed. In the case of Sakurai's object, which suffered an outburst in 1995, the entire evolution from a compact hot star to a supergiant star with RCB variability was monitored with modern telescopes, creating a convincing link between final-flash and RCB stars. However, recently Clayton et al. (2005, 2007) made the discovery that RCB stars have $^{18}O/^{16}O$ ratios that are orders of magnitude higher than those seen in any other known stars, including Sakurai's object (Geballe et al. 2002). These high ratios are inconsistent with regular stellar evolution, but can be produced in the aftermath of a merger (Clayton et al. 2007; García-Hernández et al. 2010). This finding tips the balance of evidence in favour of a merger origin for RCB stars.

RCB stars have effective temperatures in the range of 5000–7000 K, so circumstellar gas in thermodynamic equilibrium would not be able to condense into dust at distances closer than $\sim 20R_\star$. However, we observe a correlation between the pulsational phase and the onset of dust formation in five RCB stars which indicates that dust must condense close to the photosphere (Pugach 1977; Lawson et al. 1999; Crause, Lawson & Henden 2007). It is possible that shocks created by the pulsations will cause local density enhancements and encourage non-equilibrium conditions. Then the pre-conditions for carbon nucleation may be temporarily present (Goeres & Sedlmayr 1992; Woitke, Goeres & Sedlmayr 1996).

⋆Based on observations made with the Very Large Telescope Interferometer at Paranal Observatory under programme 079.D-0415.

†E-mail: stacey.bright@mq.edu.au

Such conditions existing locally over the surface of the star could allow a 'clump' of carbon dust as close as $2R_\star$ to form which is then ejected by radiation pressure. The observed time-scales for RCB dust formation fit well with those calculated by carbon chemistry models (Feast 1986; Woitke et al. 1996).

Even though all RCB stars show an infrared (IR) excess, there is no increase in the excess seen at the time of a major decline in brightness. This indicates that the amount of new dust formed in one dust formation episode is small compared to the total mass emitting around the star (Clayton 1996; Feast et al. 1997, and references therein).

Spectropolarimetry of the prototype RCB star, R CrB, obtained during a deep decline showed a change in the position angle (PA) of the continuum polarization consistent with a bipolar geometry, which includes a thick disc or torus that obscures the star and additional diffuse dust above the poles (Clayton et al. 1997). Large resolved shells with sizes ranging from 5 arcsec to 20 arcmin have been seen around various RCB stars at visible and IR wavelengths showing shapes ranging from spherically symmetric to slightly elliptical (Gillett et al. 1986; Walker 1985, 1986; Clayton et al. 1999; Clayton & Ayres 2001; Clayton, private communication).

Using near-IR interferometry, Ohnaka et al. (2003) found evidence for an asymmetrical dust geometry around R CrB at $\sim 20R_\star$ from the star in addition to a thin dust shell at 60–80$R_\star$. de Laverny & Mékarnia (2004) found an asymmetrical arrangement of dust clouds around RY Sgr in the *K* and *L* bands using adaptive optics. These dust clouds were found at ∼0.1–0.2 arcsec from the star corresponding to 700–1400$R_\star$. Asymmetrical dust was also seen at $100R_\star$ around RY Sgr in 2005 using interferometry in the mid-IR (Leão et al. 2007).

In this paper we investigate the immediate circumstellar environments of three RCB stars, RY Sgr, V854 Cen and V CrA, with the aim of determining a connection between the probable merger past of these stars and their current dust-production activities. In Section 2, we describe our observations. In Section 3, we report our modelling procedures. In Section 4, we provide the results of the modelling of the three sources, and finally, in Section 5 we discuss our results in the context of past work.

2 OBSERVATIONS

The sources were observed in 2007 June with the Very Large Telescope Interferometer (VLTI) MID-infrared Interferometric Instrument (MIDI; Leinert et al. 2003; Ratzka et al. 2007). The VLTI/MIDI interferometer operates like a classical Michelson interferometer combining the mid-IR light (*N* band, 7.5–13.5 μm) from two VLT Unit Telescopes (8.2 m). 11 observations were completed in 2007 June using two different telescope pairs (U2-U3 and U3-U4). A typical MIDI observing sequence was followed, as described in Ratzka et al. (2007). MIDI provided single-dish acquisition images with a spatial resolution of about 250 mas at 8.7 μm, flux-calibrated spectra at low and high spectral resolution ($R = 25$ and 230, respectively) and visibility curves. The spatial spectrum of the source, or the visibility function, is given by the two-dimensional Fourier transform of the sky brightness. The interferometric information along a baseline is identical to the one-dimensional (1D) Fourier transform of the curve resulting from the integration of the brightness distribution in the direction perpendicular to the baseline. The observations were performed in a high-sens mode, implying that the photometry of the sources is recorded subsequent to the fringes. We used both the grism ($\lambda/\Delta\lambda = 230$) and prism ($\lambda/\Delta\lambda = 25$) for wavelength dispersion. See Table 1 for additional details.

Table 1. VLTI/MIDI observation log.

Observation (g = grism) (p = prism)	Date	Baseline	Label	Projected baseline length (m)	Projected baseline PA (°)
RY Sgr-g	2005-06-25	U1-U4	B_1	122	34
RY Sgr-g	2005-06-25	U1-U4	B_2	123	36
RY Sgr-g	2005-06-25	U1-U4	B_3	128	65
RY Sgr-g	2005-06-26	U1-U4	B_4	125	68
RY Sgr-g	2005-05-26	U3-U4	B_5	57	98
RY Sgr-g	2005-06-28	U3-U4	B_6	62	110
RY Sgr-g	2005-06-26	U3-U4	B_7	57	135
RY Sgr-g	2007-06-29	U2-U3	B_1	47	32
RY Sgr-g	2007-06-29	U2-U3	B_2	41	54
RY Sgr-g	2007-06-29	U2-U3	B_3	34	58
RY Sgr-g	2007-06-30	U3-U4	B_4	55	94
RY Sgr-g	2007-06-30	U3-U4	B_5	59	129
V CrA-p	2007-06-29	U2-U3	B_1	45	45
V CrA-p	2007-06-29	U2-U3	B_2	32	63
V CrA-p	2007-06-30	U3-U4	B_3	53	89
V CrA-p	2007-06-30	U3-U4	B_4	61	128
V854 Cen-g	2007-06-30	U3-U4	B_1	60	101
V854 Cen-p	2007-06-30	U3-U4	B_2	56	153

Note: Results of the RY Sgr observations taken in 2005 were published by Leão et al. (2007).

The image acquisition field of view is 3 arcsec. A 'chopped' image is produced by tilting the secondary mirror off-centre and taking an image of the sky followed by an image being taken at the centre position. This process of tilting back and forth is done rapidly several times. The resulting images are subtracted to cancel the sky background leaving an image with only the source signal. This image is used to position the sources to a pre-determined pixel in order to maximize the overlap of both images for the interferometric measurements. The MIDI images have a clear Airy pattern and the full width at half-maximum (FWHM) is consistent with the source being unresolved at 8.7 μm, with an angular diameter of <150–200 mas, given the error bars. In absence of this nodding technique, the quality of the image is limited and the dynamics are restricted to about 2–3 per cent of the flux at peak.

Next, the beam combiner and the dispersive device are inserted, producing two interferometric beams of opposite sign. The zero optical path difference (OPD) is searched for by scanning around the expected point of path-length equalization. Once the OPD is found, the interferometric measurements start using self-fringe-tracking. A temporal fringe pattern is produced by scanning constantly at a range of OPD = 40–80 μm typically in steps of 2 μm.

We used two different MIDI data reduction packages: MIA developed at the Max-Planck-Institut für Astronomie and EWS developed at the Leiden Observatory (MIA+EWS,[1] V.1.5.1). MIDI spectra were calibrated using the stars HD 152334 (K4III 3.99 ± 0.07 mas), HD 163376 (M0III 3.79 ± 0.12 mas), HD 169916 (K1III 3.75 ± 0.04 mas) and HD 177716 (K1III 3.72 ± 0.07 mas). The accuracy of the absolute flux calibration is better than 10 per cent. The observation log is given in Table 1.

As the photometry of individual telescopes is recorded a few minutes after the fringe recording, the fluctuations of the atmosphere affect the absolute level of the visibilities at the 8–15 per cent

[1] Available at http://www.strw.leidenuniv.nl/~nevec/MIDI/index.html

level (depending on the atmospheric conditions). This is by far the worst source of error in this mode. Because the knowledge of the level of the fluctuations is lacking, it is not possible to easily decrease this error. Furthermore, the error affects all the disperser channels almost identically and are hence highly correlated with the atmospheric error. There are also other sources of noise that affect the spectral channels independently at a level of three to five times lower than the atmospheric error. These include the photon noise and the mismatches of the beam overlap effect. This implies that the differential information contained in the slope of the dispersed visibility curve is more tightly constrained than the absolute level. This mix of correlated and uncorrelated errors makes any model fitting using the classical approach of the reduced χ^2 ill-suited. However, our reduced χ^2 remains an appropriate indicator of the fit at first approximation and will be used to compare several models.

Differential phase measurements are provided by MIDI and are well suited to detect source asymmetry; however, they have limitations. The phase extracted is the departure of the spectral phase compared to the expected phase of the fringes given that the OPD is known. As a differential measure, the absolute phase is not recovered in the data reduction process. Moreover, the slope of the differential phase is also removed. As a consequence, the differential phase is mostly sensitive to complex objects composed of at least two sources exhibiting very different spectral signatures within the *N* band, or sources with large variations of the phases, such as well-resolved binary sources (e.g. Ratzka et al. 2009). As such, it is particularly well suited for the study of bright stellar sources surrounded by dusty discs (e.g. Deroo et al. 2007; Ohnaka et al. 2008). We did not detect such a large amplitude phase signal for the two reasons presented above, namely the spectral changes of the differential phase induced by the presence of the clumps are too slow and strongly decreased in the reduction process and the spectral signature of the clumps does not differ significantly enough to induce a large spectral signature that would provide a definite signature. Therefore, we are not able to use the differential phases for a direct proof of asymmetries in the circumstellar material around the RCB stars.

Spitzer Infrared Spectrograph (IRS) short-low (SL) and long-low resolution spectra of V854 Cen and V CrA were obtained from the *Spitzer* archive. An existing IRS spectrum of RY Sgr is heavily saturated and was not used in our analysis. The V854 Cen spectrum was obtained on 2008 August 12 and the V CrA spectrum was obtained on 2005 September 14. The spectra were re-reduced using the SMART software package as described in Furlan et al. (2006). *Infrared Space Observatory* (*ISO*) spectra taken with the Short Wavelength Spectrometer (SWS) were obtained for RY Sgr (1997 March 25) and V854 Cen (1996 September 9) (Lambert et al. 2001). These data were obtained from the *ISO* archive and were re-reduced using a slightly modified version of the SWS routines developed by Sloan et al. (2003). A low signal-to-noise ratio *ISO* spectrum of V CrA is present in the archive but was not used in our analysis. An observation log of the *ISO* and *Spitzer* spectra is given in Table 2. Light curves using the American Association of Variable Star Observers (AAVSO) and All Sky Automated Survey (ASAS) photometry for the three RCB stars are presented in Section 5.

Table 2. *ISO* and *Spitzer* observation log.

Star	Instrument/telescope	Date
RY Sgr	SWS/*ISO*	1997-03-25
V CrA	IRS/*Spitzer*	2005-09-14
V854 Cen	SWS/*ISO*	1996-09-09
V854 Cen	IRS/*Spitzer*	2008-06-12

3 MODELLING OF THE DUSTY ENVIRONMENTS

Extensive modelling is needed to understand the RCB star environments. Model parameters can be better constrained if many observations across the *uv* plane are obtained. Observations were taken across different baselines and PAs for each star as seen in Fig. 1, and a few visibility measurements for each object were obtained.

Two approaches are used in order to model the data. First, following the approach published by Leão et al. (2007), we use several geometric models to account for the dispersed visibilities, first obtaining a monochromatic fit and then seeking for a wavelength-dependent (chromatic) solution. The geometrical models provide information on departure from spherical symmetry in the circumstellar environment. Secondly, we use the 1D radiative transfer

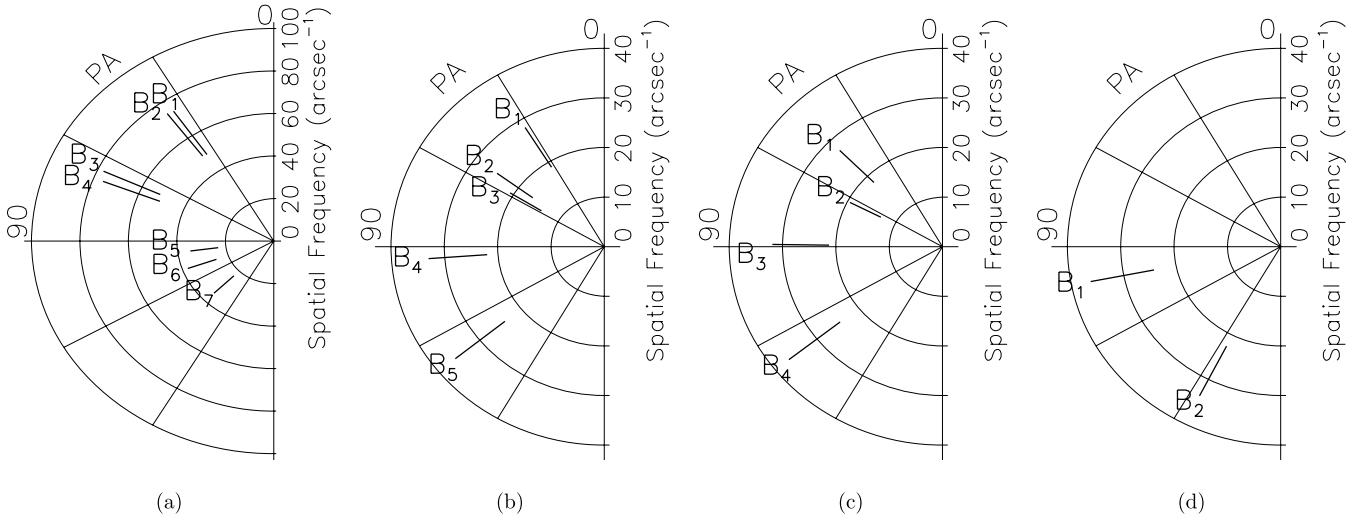

Figure 1. Charts of the *uv* plane for (a) RY Sgr in 2005, (b) RY Sgr in 2007, (c) V CrA and (d) V854 Cen are shown, representing their projected baseline lengths and PAs with the same labels as in Table 1. Note the increased spatial frequency range for RY Sgr in 2005 data compared to the 2007 observations.

code, DUSTY, a public-domain simulation code that models radiation transport in a circumstellar dusty environment. DUSTY analytically integrates the radiative-transfer equation in plane-parallel or spherical geometries (Ivezic, Nenkova & Elitzur 1999; Ivezic & Elitzur 1997). DUSTY provides a realistic view of the source, as it uses both the dispersed visibilities and the spectral energy distribution (SED) of the source. However, DUSTY does not provide any information on departure from spherical symmetry.

The two modelling approaches are complementary, provided that one ensures broad agreement in the areas of overlap. For our models, described in detail in Section 4, this agreement is sought between the geometrical and DUSTY models of the shells only.

3.1 Geometrical fitting

If the circumstellar material is spherically symmetric, each sampling with baselines of similar projected lengths but different PAs will produce the same visibility curve. However, the data show that this is not the case despite the limited number of baselines considered, particularly in the case of RY Sgr. Therefore, models are used to interpret the visibility curves and determine the possible geometry of the circumstellar material. In our geometrical models, we consider different combinations of the following structures: a central point source representing the star, a Gaussian shell of dust around the star (i.e. a circular structure with a Gaussian light distribution), a circular, uniform dusty disc around the star, a non-centrosymmetric, elliptical dusty disc around the star (because of the simplicity of our models, this could represent either a circular disc observed at an angle of inclination or an actual elliptical disc observed face-on) and a second point source representing a dust 'cluster' near the star. Typically, RCB stars are not thought to have homogeneous dust shells, so in our models a 'shell' represents an approximate spherical distribution of clumps that are individually unresolved. The physical interpretation of the second point source (the cluster) is an estimate for the level of asymmetry in the distribution of dust clumps surrounding the RCB star. As our data were collected with telescope pairs, closure phase information was not obtained and therefore there is an ambiguity of 180° in the position of the cluster.

If one obtains observations that employ only short VLTI baselines, the *uv* plane coverage is limited. Therefore, the fits from our geometric models are only indicative of what may be surrounding the RCB star, as the models are not unique. Nevertheless, the extent of model degeneracy was tested by extensive exploration of parameter space.

At the start of our fitting procedure, we neglect any variation of the morphology as a function of wavelength. Every combination of structures modelled results in a set of monochromatic visibility curves. This approach gives us a basic understanding of the global morphology of the object. The value of the reduced χ^2 is minimized for all the baselines. Only the errors in the mean visibility level are considered. The parameters of the monochromatic models are listed in Table 3 and results presented in Sections 4.1.1, 4.2.1 and 4.3.1.

Because the differential information contained in the slope of the dispersed visibility is more tightly constrained than the absolute level (see Section 2), our analysis relies heavily on the shapes of the dispersed visibility curves rather than the absolute level of the visibility curves. Therefore, it is not surprising that we obtain some reduced χ^2 values less than 1 for our models. In this context, a reduced χ^2 value of 0.2 remains better than a reduced χ^2 value of 0.8 for the same model, as it means that the dust shell density distribution is better accounted for.

Next, a chromatic analysis of visibilities across all wavelengths is performed. The separation of the cluster from the star and its PA is assumed to be the same at all wavelengths. However, the FWHM of the shell and the flux of all components are wavelength dependent and are therefore adjusted to fit wavelength-dependent visibility curves. Results of the chromatic fits for RY Sgr are presented in Section 4.1.1. Fits were also completed for V854 Cen and VCrA, but are not presented in this paper as they did not provide adequate information. Specific results of the geometrical fitting for each RCB star are presented in Section 4.

Table 3. Parameters of the monochromatic geometric fits to the visibility curves. The models are as follows: PS: point source; UD: uniform disc; G: Gaussian shell (representing a spherical distribution of clumps that are individually unresolved); C: cluster (an off-centred point source representing an asymmetry in the distribution of dust clumps with an ambiguity of 180°) and EUD: elliptical uniform disc (with different major and minor axes).

Star (epoch)	Model	$\chi 2$	Flux PS (per cent)	Flux shell/disc (per cent)	FWHM[a] (mas)	Diam disc[b] (mas)	Flux cluster (per cent)	Sep of cluster (mas)	PA[c] (°)
RY Sgr (2005)	PS + UD	1.7	0.21	0.79	–	33	–	–	–
RY Sgr (2005)	PS + G + C	0.31	0.11	0.8	18	–	0.09	15	79
RY Sgr (2005)	PS + EUD	1.1	0.2	0.8	–	18, 13	–	–	79
RY Sgr (2007)	PS + G	14	0.05	0.95	36	–	–	–	–
RY Sgr (2007)	PS + UD	12	0.17	0.83	–	46	–	–	–
RY Sgr (2007)	PS + G + C	1.3	0.15	0.74	37	–	0.11	25	175
RY Sgr (2007)	PS + UD + C	1.8	0.19	0.63	–	58	0.18	23	172
RY Sgr (2007)	PS + EUD	2.7	0.17	0.83	–	36, 19	–	–	178
V CrA	PS + G	0.81	0.56	0.44	46	–	–	–	-
V CrA	PS + UD	0.73	0.60	0.4	–	70	–	–	-
V CrA	PS + G + C	0.26	0.55	0.4	45	–	0.05	84	16
V CrA	PS + UD + C	0.27	0.61	0.34	–	76	0.05	100	9
V CrA	PS + EUD (a)[d]	0.41	0.58	0.42	–	180, 52	–	–	166
V CrA	PS + EUD (b)[d]	0.61	0.59	0.41	–	96, 63	–	–	177
V854 Cen	PS + G	0.58	0.16	0.84	24	–	–	–	–
V854 Cen	PS + G + C	0.8	0.3	0.6	24	–	0.1	33	40

[a]FWHM of the Gaussian shell; [b]diameter of UD or major axis, minor axis of EUD; [c]PA of cluster or orientation of EUD; [d]two PS + EUD models for V CrA with different major and minor axes that produce similar results.

3.2 DUSTY fitting

DUSTY utilizes the self-similarity and scaling relations of the radiatively heated dust, for example the shell is uniquely characterized by its optical depth. This means that absolute values (synthetic surface brightness, flux and visibility) are not uniquely determined by the transfer problem and must be inferred by external constraints – in our case, the stellar luminosity and distance.

DUSTY requires seven main input parameters: the temperature of the central star, the chemical composition of the dust grains, the grain size distribution, the density distribution of the dust, the temperature of the dust at the inner radius, the overall radial optical depth at a given wavelength and the thickness of the dust shell. DUSTY's outputs consist of a detailed SED, the detailed surface brightness at our specified wavelengths (8–13 μm), tables of the radial profiles of density, optical depth and dust temperature, and visibility as a function of the spatial frequency for the specified wavelengths. The synthetic visibility profiles throughout the *N* band (7.5–13 μm) are generated using a set of 15 wavelengths. These are compared with the observed MIDI visibilities for each baseline.

Because DUSTY is a 1D radiative transfer code, it is unable to model non-spherically symmetric, non-homogeneous (clumpy) structures. As a result, the observed visibility curves that present evidence for asymmetric geometric structures cannot be reproduced accurately by the DUSTY models. On the other hand, since radiative transfer is taken into account, DUSTY can model the characteristics of the circumstellar dust (such as producing an SED) in ways that the geometric models cannot. The input parameters for the DUSTY models are given below.

(i) The temperature and the spectrum of the central star are constrained by model fitting, assuming a simple blackbody source. The effective temperatures are based on Asplund et al. (1998, 2000).

(ii) The dust is made entirely of amorphous carbon. This is the common assumption for these hydrogen-deficient stars (Lambert et al. 2001). DUSTY uses standard optical constants for amorphous carbon from Hanner (1988).

(iii) A Mathis–Rumpl–Nordsieck (MRN) size distribution (Mathis, Rumpl & Nordsieck 1977) is assumed: $n(a) \propto a^{-q}$ for $a_{\rm min} \leq a \leq a_{\rm max}$. For our analysis, we used $q = 3.5$ and varied $a_{\rm min}$ and $a_{\rm max}$ (see Section 5.5).

(iv) Inside the shell, the density follows an r^{-P} distribution as in a steady-state wind with constant velocity. The power exponent, *P*, was the easiest parameter to constrain and as such was normally the first parameter chosen when fitting the SED and visibility curves. A larger value causes most of the dust grains to concentrate near the inner radius ($R_{\rm inner}$). When grains are concentrated near $R_{\rm inner}$, they absorb a number of photons causing a 'screen' to form (this is especially apparent with smaller grains which absorb more efficiently). The extent of this screen dramatically affects the slope of the visibility curve. Therefore, a larger value of *P* typically yields a steeper slope in the modelled visibility curves.

(v) The temperature of the dust at the inner rim of the shell ($T_{\rm inner}$) is chosen individually for each star and mainly constrained by the SED. A higher temperature chosen here causes a larger IR emission.

(vi) The optical depth, τ_V, is chosen so as to match the *V* band (0.55 μm) photometric measurement of the star. Like $T_{\rm inner}$, a higher τ_V causes more flux in the IR.

(vii) The thickness of the dust shell ($R_{\rm out}/R_{\rm in}$) is constrained mainly by the visibility curve but does not have a large effect. Once a certain thickness is reached the output visibility curves do not change noticeably until a thickness ratio of ∼90–100 is reached, at which point the object becomes over-resolved. Therefore, the smallest shell thickness that gives the best result is chosen, but this parameter is poorly constrained.

Table 4. RCB target stars; basic characteristics.

Star	M_V[a] (mag)	A_V[b] (mag)	V[b] (mag)	$T_{\rm eff}$[c] (K)	D (pc)
RY Sgr	−5	0.06	6.4	7250	1800
V CrA	−4	0.37	9.9	6250	5200
V854 Cen	−4.5	0.00	7.1	6750	2100

[a] Alcock et al. (2001) and Tisserand et al. (2009); [b] from Lawson et al. (1990); [c] from Asplund et al. (2000).

In order to ease the comparison between the shell produced by DUSTY models and that produced by the geometrical models, a Gaussian curve is fitted to the 1D collapsed intensity distributions of the best DUSTY model at a chosen wavelength (9 μm). The half width at half-maximum (HWHM) of the DUSTY Gaussian fit (from here on called $R_{\rm DUSTY}$) is used as the distance to the shell in our analysis to make comparison easier.

As discussed, DUSTY does not take into account the distance nor the luminosity of the star, so the user must scale DUSTY results to specific stars. The distances are calculated from the M_V, A_V and V values in Table 4, and the luminosity inputs are kept within the range of RCB stars with these parameters. The results are also corrected for the standard Cardelli–Clayton–Mathis (CCM) reddening law (Cardelli, Clayton & Mathis 1989) using an input of $E(B-V)$, where $E(B-V) = A_V/3.1$. The scaling process results in a stellar radius and inner shell radius in physical units. The inputs and outputs, including the reduced χ^2, are displayed in Table 5. Specific results of the DUSTY fitting for individual stars are discussed in Section 4.

4 RESULTS

4.1 RY Sgr

4.1.1 Geometrical fitting

Using the geometrical models described in Section 3.1, we find that the best monochromatic model (with the lowest reduced χ^2) for the RY Sgr 2007 data set is a combination of a central star, a Gaussian dust shell and a dust cluster (see Fig. 2).

A significant wavelength dependence of the model parameters was found for the 2007 data set (see Fig. 2). The FWHM of the envelope grows with increasing wavelength and is accompanied by a flux increase in both the star and the cluster. Such a behaviour is counter-intuitive. In depth investigations of the degeneracy between the flux and size parameters were first performed by forcing the flux of the envelope to increase with the wavelength and secondly by allowing the cluster position to be free. After a large exploration of the parameter space, a good parameter set was not found. Next, a more simple geometrical model, involving a stellar unresolved source and a Gaussian dust shell, was tested. In this case, the flux of the envelope increased with wavelength, but the fit was not satisfactory (reduced $\chi^2 = 12$). To summarize, the strongly suspected asymmetries in the 2007 data can be ascribed, at first order, by the presence of a cluster; however, the model has some problems. 'Clusters' introduce a spectrally dependent sinusoidal pattern in the

Table 5. DUSTY model inputs and outputs.

Star	Input parameters								Output results			
	$T_{\rm eff}$ (K)	P^a	$T_{\rm inner}{}^b$ (K)	τ_V	$\frac{R_{\rm out}}{R_{\rm in}}{}^c$	D (pc)	L ($L_\odot$)	$E(B-V)$	$R_\star$ ($R_\odot$)	$R_{\rm in}{}^d$ (mas), ($R_\star$)	$R_{\rm DUSTY}{}^e$ (mas), ($R_\star$)	$\chi^{2\,f}$
RY Sgr (2005)	7250	3.3	900	1.2	50	1800	8700	0.02	59	7, 48	13, 79	1.9
RY Sgr (2007)	7250	2.7	1000	1.0	50	1800	8700	0.02	59	9, 57	17, 108	0.6
V CrA	6250	1.7	1000	1.5	30	5200	4500	0.12	57	2, 41	5, 100	1.3
V854 Cen	6750	2.7	1075	0.45	50	2100	8200	0	66	6, 38	11, 71	4.3

[a]Dust density is r^{-P}; [b]$T_{\rm dust}$ at $R_{\rm inner}$; [c]shell thickness in multiples of $R_{\rm inner}$;
[d]shell inner radius; [e]HWHM of the DUSTY geometrical Gaussian fit at 9 μm; [f]reduced χ^2 of visibility fits for a subset of baselines only (see text, Section 4).

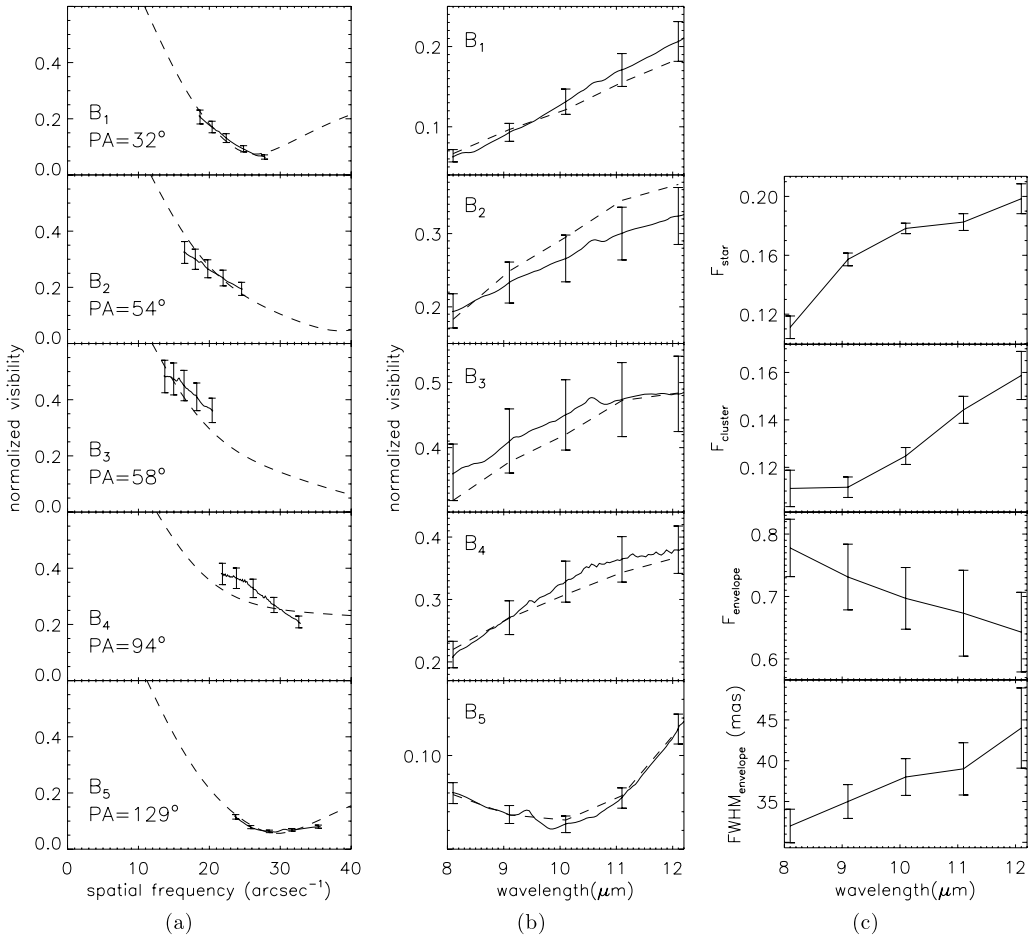

Figure 2. Geometrical fits (dashed line) for RY Sgr in 2007 are shown using a model consisting of a point source, a Gaussian shell and a cluster. (a) The fits using the monochromatic models are shown. (b) Fits using the chromatic models are shown. (c) Corresponding chromatic quantities derived from the best-fitting model. Each panel is labelled by the baseline and PA referenced in Table 1 and Fig. 1. The observed visibility curves (solid lines) have indicative error bars marked.

dispersed visibility curves which is only partially probed by our limited data set.

There is a difference in behaviour between the 8–9 and 9–12 μm spectral regions that may reflect different opacity regimes, with a decreasing opacity at a larger wavelength explaining the higher star and cluster relative fluxes and also an increase of the contribution of the cooler and more extended parts of the envelope.

4.1.2 *DUSTY fitting*

DUSTY can only account for the broad characteristics of the dust shell and is unable to provide any information on asymmetries detected. In 2005, the longer baselines (B_1, B_2, B_3, B_4) probe the smaller structures (i.e. closer to the star) and show strong evidence of a cluster (see Fig. 3). Therefore, these baselines cannot be accurately fitted with DUSTY. In contrast, the short baselines (B_5, B_6, B_7) should detect the symmetrical Gaussian shell and can theoretically be fitted with DUSTY. However, a departure from symmetry is clearly seen when comparing B_5 and B_7. Both baselines share the same length, but have different PAs. Of course, if the circumstellar material was spherically symmetric these measurements would produce the same visibility, but B_7 has a significantly higher visibility than B_5. This implies that an asymmetry also exists at larger scales around the star (see Leão et al. 2007). As a result, the reduced χ^2 values for

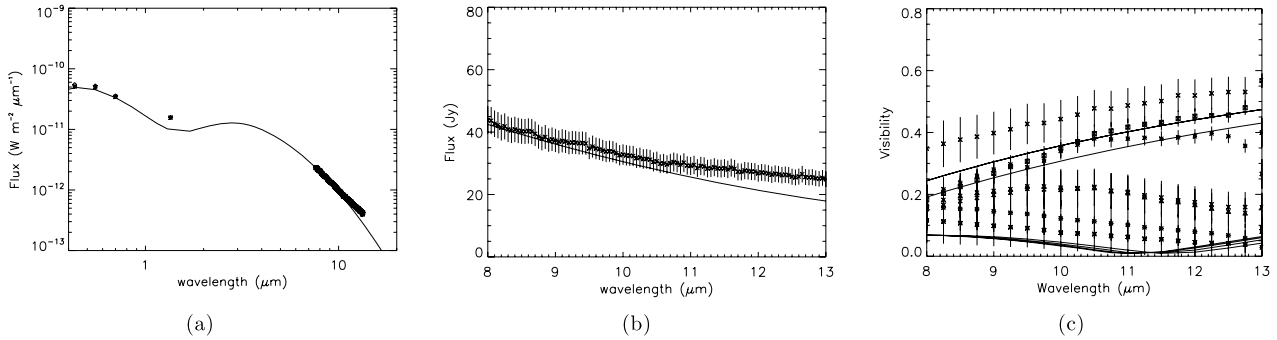

Figure 3. Best DUSTY fits for RY Sgr in 2005. (a) The modelled SED (solid line) is shown along with the observed spectra (symbols). (b) Only the MIDI spectrum (crosses) is shown with the model (solid line). (c) The seven baseline visibility curves (symbols) are shown with the visibility fits (solid line). The visibility curves are shown from the shortest baseline (top) to the longest baseline (bottom). Note that only B_5 and B_6 can be fitted. The other baselines, B_1, B_2, B_3, B_4, B_7, show strong evidence of asymmetry which DUSTY cannot account for (see Section 4.1.1). Indicative error bars are marked.

the RY Sgr (2005) DUSTY fits (presented in Table 5) are calculated from only the B_5 and B_6 visibility curves.

In 2007, only short baseline observations were obtained. These can be fitted relatively well with DUSTY, although B_4 and B_5 show a hint of asymmetry (see Fig. 4). This agrees with the asymmetry found with the geometrical models. The reduced χ^2 values for the DUSTY fits are based only on the visibility curves of the three shortest baselines. It is interesting to note that the position of the cluster inferred with good confidence in 2005 and the other suspected in 2007 both lie close to the dust shell inner rim inferred from the DUSTY modelling. DUSTY placed the dust shell ($R_{\rm DUSTY}$) at ∼13 mas in 2005 and 17 mas in 2007. These values are the same, within the uncertainties, as the dust shell inner rim found with the geometrical models (∼9 mas in 2005 and 18 mas in 2007).

4.2 V CrA

4.2.1 Geometrical fitting

Similar to RY Sgr, the geometrical models for V CrA reveal that the visibility curve of this source is best fitted by a combination of a central star, a shell and a dust cluster (see Fig. 5). We find the separation of the cluster and the star to be 84 mas (437 au, using a distance of 5200 pc) and the PA of the cluster to be 16°. The radius of the Gaussian shell is 22 mas. This places the cluster about four times farther away than the shell's radius. In addition, the dust cluster has a flux of only 5 per cent of the total system flux. However, all the geometrical models for V CrA provide a similar reduced χ^2. Therefore, the inclusion of a cluster is not clearly justified by the data.

4.2.2 DUSTY fitting

Good DUSTY fits for V CrA were produced for the SED and four visibility curves. The consistency between the visibility curves and the SED suggests that the large estimated distance to V CrA (5200 pc) is appropriate. The consistency may also suggest that a spherical shell surrounding the star may be an appropriate model for V CrA. However, because V CrA is so far away, it is not the best object to detect asymmetries in the circumstellar environment. The general shape of the target can be seen, but the inner circumstellar regions where asymmetries are more likely to be found cannot be resolved.

DUSTY places the dust shell ($R_{\rm DUSTY}$) at 5 mas. Unlike RY Sgr, this is significantly smaller than the inner rim predicted by the geometrical models for V CrA (∼20 mas). The DUSTY fits to the V CrA data are found in Fig. 6.

4.3 V854 Cen

4.3.1 Geometrical fitting

For V854 Cen, only two baselines were obtained. As a result, the geometrical fits are highly degenerate. In addition, because the baselines obtained are short, they only probe the larger scale structure or the larger shell portion of V854 Cen. Therefore, we used only the two most basic models, a Gaussian shell and a Gaussian shell plus

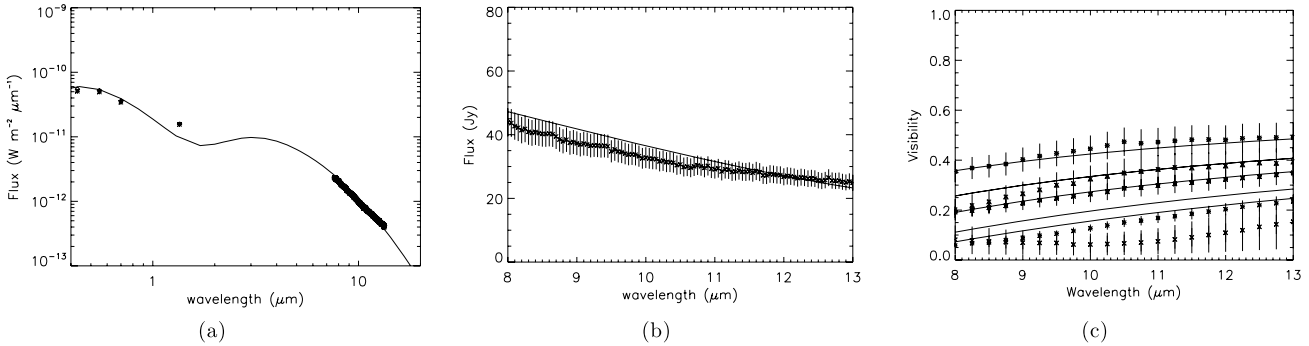

Figure 4. Best DUSTY fits for RY Sgr in 2007. (a) The modelled SED (solid line) is shown along with the observed spectra (symbols). (b) Only the MIDI spectrum (crosses) is shown with the model (solid line) (c) The five baseline visibility curves (symbols) are shown with the visibility fits (solid line). The visibility curves are shown from the shortest baseline (top) to the longest baseline (bottom). Note that only the three longer baselines (B_1, B_2, B_3) can be fitted (see Section 4.1.1) Indicative error bars are marked.

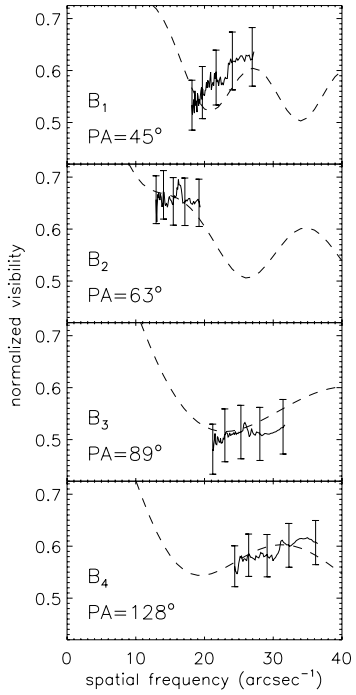

Figure 5. Monochromatic geometrical fits (dashed line) for V CrA using a model consisting of a point source, a Gaussian shell and a cluster.

cluster to fit the two baselines (see Table 3). However, the visibility curves for the two fits are too similar to determine if there is any asymmetry. We therefore only use the Gaussian shell fit for our analysis (see Fig. 7). This places the FWHM of the Gaussian shell at 24 mas with a flux comprising 84 per cent of the total system.

4.3.2 *DUSTY fitting*

Good DUSTY fits for V854 Cen are obtained for the two baselines, and asymmetries are not implied from the fits obtained. But at ∼8 and ∼11.5 μm, an emission feature is seen, in both the SED and the visibilities, that causes the model to deviate from the observations. These features are discussed in more detail in Section 5.

DUSTY places the dust shell at 11 mas ($R_{\rm DUSTY}$). This is similar to the inner rim predicted by the geometrical models for V854 Cen (12 mas). The DUSTY fits to the V854 Cen data are found in Fig. 8.

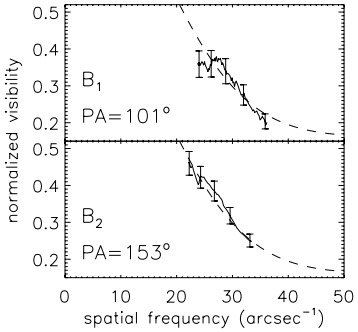

Figure 7. Monochromatic geometrical (dashed line) fits for V854 Cen using a model consisting of a point source and a Gaussian shell.

5 DISCUSSION

5.1 Dust formation frequency

Our observations, in combination with optical light curves, may shed light on the frequency and location of dust formation in RCB stars. Current knowledge suggests that dust forms in clumps at discrete locations around RCB stars, and a visible light decline will be observed if a clump is ejected in the line of sight. Therefore, declines in the light curve will not necessarily correspond to structure observed by the VLTI. Furthermore, if a clump is ejected towards us, causing a decline in the visual light curve, it is unlikely to be detected by the VLTI. Conversely, a clump that is easily detected by the VLTI is likely to be one that was not ejected towards us and therefore did not produce a light curve decline. On the other hand, RCB stars are known to undergo periods of inactivity, where the star is at maximum light sometimes for years, and periods of strong activity, when the star is constantly declining and recovering (Clayton 1996). Because of this, we presume that the clusters we resolve were likely produced during a period of high dust-production activity that also resulted in light declines.

Using the distance to each of our RCB stars and their stellar radii, as well as an average dust outflow velocity of 300 km s^{-1}, we estimate the time it takes a dust clump to reach the observed dusty shell ($R_{\rm DUSTY}$; see Section 3.2) after initial ejection, assuming the dust forms at $2R_\star$ (Clayton et al. 1992; Clayton, Geballe & Bianchi 2003). As discussed in Section 3.1, the geometrical cluster represents a break from symmetry in the distribution of dust clumps of the shell, but does not necessarily indicate the position of a particular clump. Therefore, we use the simplistic $R_{\rm DUSTY}$ as the distance for an individual clump to travel for our analysis. We also

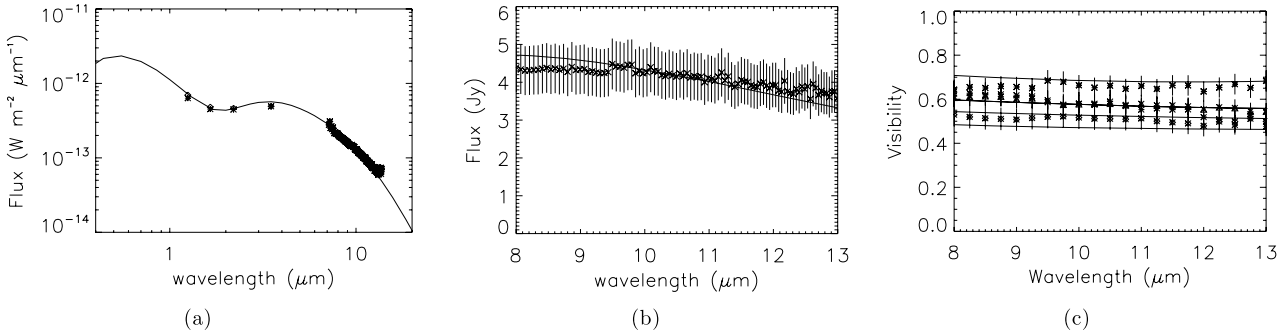

Figure 6. Best DUSTY fits for V CrA. (a) The modelled SED (solid line) is shown along with the observed spectra (symbols). (b) Only the MIDI spectrum (crosses) is shown with the model (solid line). (c) The four baseline visibility curves (symbols) are shown with the visibility fits (solid line). The visibility curves are shown from the shortest baseline (top) to the longest baseline (bottom). Indicative error bars are marked in each figure.

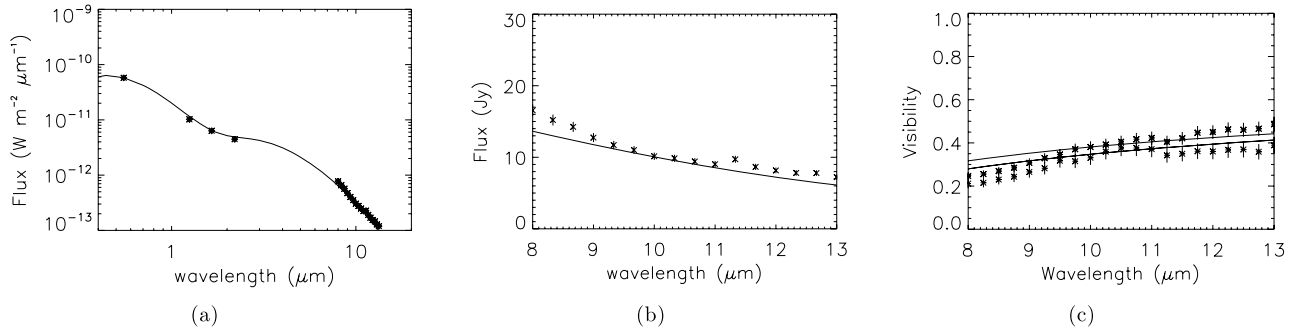

Figure 8. Best DUSTY fits for V854 Cen. (a) The modelled SED (solid line) is shown along with the observed spectra. (b) Only the MIDI spectrum (crosses) is shown with the model (solid line). (c) The two baseline visibility curves (symbols) are shown with the visibility fits (solid line). Indicative error bars are marked in each figure. At ∼8 and 11.5 μm, we see evidence of two extended emission features.

Table 6. Time for dust to reach shell and mass of shell.

Star	$R_{\rm DUSTY}$ (mas), ($R_\star$)	t^a (months)	Pulsational period (d)	$M_{\rm shell}$ ($M_\odot$)	$n_{\rm clumps}$
RY Sgr (2005)	13, 79	5	38[b]	3.7×10^{-7}	37
RY Sgr (2007)	17, 108	7	38[b]	3.7×10^{-7}	37
V CrA	5, 100	5	57[c]	6.5×10^{-7}	65
V854 Cen	11, 71	5	43[b]	1.4×10^{-7}	14

[a] Time to reach $R_{\rm DUSTY}$, see Section 3.2; [b]from Crause et al. (2007); [c]from Lawson et al. (1990).

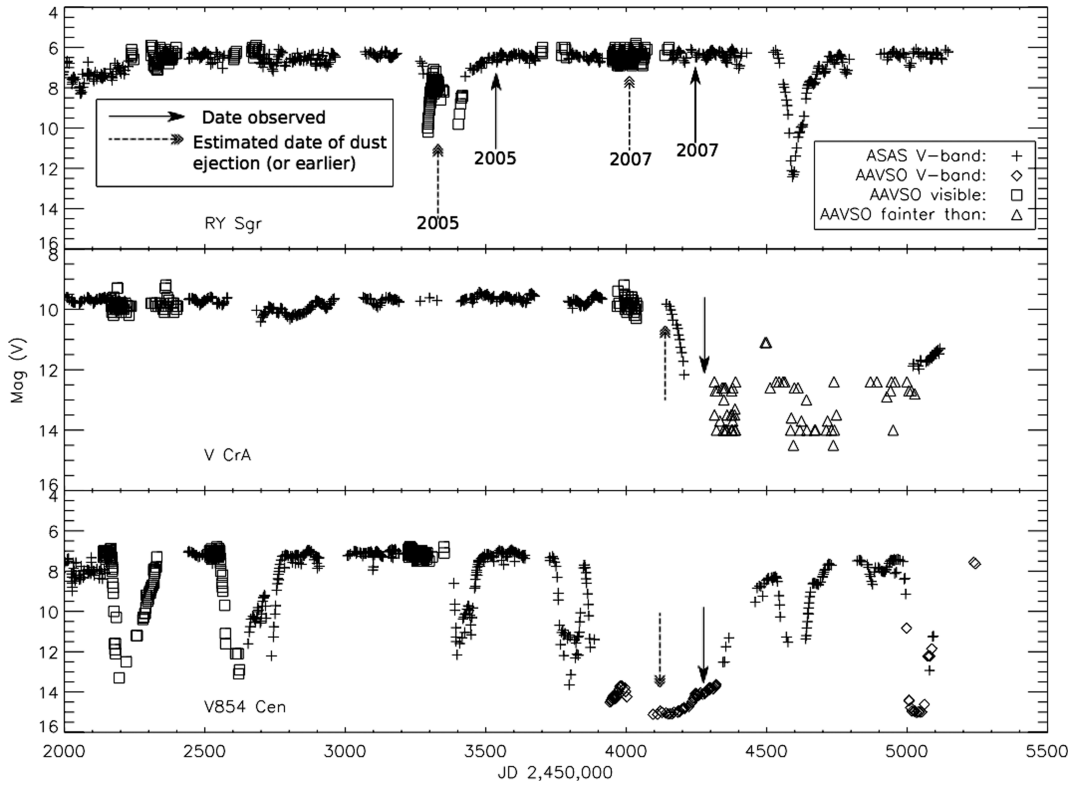

Figure 9. Light curves for RY Sgr (upper), V CrA (middle) and V854 Cen (lower), from 2001 April to 2010 January are shown. Our VLTI observations took place in 2005 June (RY Sgr; JD 245 3550) and 2007 June (RY Sgr, V CrA and V854 Cen; JD 245 4275). Estimated dates when the observed dust was ejected are marked with arrows. The intervals between ejection and observation should be considered lower limits.

assume that all the dust leaves the star in the plane of the sky; therefore, this estimated time-scale is actually a lower limit. Table 6 lists $R_{\rm DUSTY}$ and a lower limit of the time it takes the dust to reach $R_{\rm DUSTY}$ for each of our RCB stars.

V band light curves of our RCB stars are plotted in Fig. 9 using data from ASAS-3 (Pojmanski 2002) and the AAVSO. The 2005 and 2007 VLTI observations of RY Sgr were obtained on JD 245 3550 and JD 245 4275. Dust was observed at 13 and 17 mas

(24 and 31 au; see Table 5) in 2005 and 2007, respectively. It will take a minimum of 5 and 7 months for the dust to reach these distances. 5 months prior to the 2005 VLTI observation, when the dust was expected to be ejected, there is a decline in the light curve (JD 245 3330). However, 7 months prior to observation of RY Sgr in 2007 (JD 245 4065), when the dust was expected to be ejected in 2007, there is no visual decline. There are no declines during the period of JD 245 3550–245 4500.

Dust was observed at 5 mas (1 au) around V CrA in 2007. It would take at least 5 months from ejection to reach this distance. Looking at the light curve 5 months prior to our observation (JD 245 4130), V CrA is just beginning a visual decline after a long period of inactivity (at least 7 yr). While the light curve shows relative inactivity prior to this time (especially compared to V854 Cen), V CrA still has significant IR emission. This could be an indication that dust around V CrA is actively forming in a plane that is not in our line of sight.

Dust was observed at 11 mas (5 au) around V854 Cen in 2007. It would take at least 5 months from ejection to reach this distance. 5 months prior to our observation (JD 245 4130), V854 Cen is in the middle of an extremely active dust-production period, such that the observed dust cluster is likely to be related to those that are obscuring our line of sight.

Without additional epochs of VLTI observations of these RCB stars, covering a significant time period, it is difficult to reconstruct the dust-production frequency and history of these objects. But it is clear from our analysis that observations such as these, taken over time, combined with IR and visible brightness variations, could allow us to determine the time and location of dust production in these objects.

5.2 Dust mass

MOCASSIN, a 3D Monte Carlo code (Ercolano, Barlow & Storey 2005), was used to model the radiative transfer in the shells surrounding our three RCB stars, resulting in fits to the three MIDI SEDs. (Note that the RY Sgr MIDI 2005 and 2007 data were identical within 5 per cent, so only the 2007 data are used in this paper.) The same input parameters were used as in the DUSTY fits listed in Table 5. Using MOCASSIN, we find that the dust shells have an average mass of $\sim 4 \times 10^{-7}$ $M_{\odot}$. Clayton et al. (1992) estimated that a single ejected clump has a mass of $\sim 10^{-8}$ $M_{\odot}$. Therefore, using a simplified calculation, we find that for each shell to grow in mass to 4×10^{-7} $M_{\odot}$ it has to contain approximately 40 individual clumps. The time it takes to accumulate this amount of mass may be estimated by using the pulsational period of the RCB stars.

The onset of dust formation has been found to be correlated with the pulsational phase in five RCB stars, including RY Sgr and V854 Cen (Pugach 1977; Lawson et al. 1999; Crause et al. 2007). RCB stars' pulsation amplitudes are at most a few tenths of a magnitude and their periods are 40–100 d (Lawson et al. 1990; Lawson & Cottrell 1997). If one clump is ejected every pulsation period (or roughly every 50 d), it will take $\sim$5 yr to build a shell with the typical observed masses. If the dust expands at 300 km s^{-1}, a clump will be at $\sim 800 R_{\star}$ from the star after 5 yr, which is well within the highly unconstrained, outer shell radius estimated by DUSTY, $\sim 3000 R_{\star}$ (assuming, as before, $R_{\rm DUSTY} = 10$ mas and a distance of 2000 pc). Table 6 contains specific calculations for our RCB stars, including the pulsation period for each star, the mass of its shell and the number of clumps within the shell.

5.3 Dust geometry

Looking at our DUSTY results in connection with the light curves, the time it takes for ejected dust to travel to $R_{\rm DUSTY}$ (see Table 6), and the dust shell mass, we find that, overall, our observations are consistent with dust forming in clumps ejected randomly around the star so that over time they may create a spherically symmetric distribution of dust. But we also must look to our geometrical models to determine if there is an overall preferential dust ejection axis or plane.

The geometrical fits (see Section 4 and Table 3) show evidence for asymmetry in the dust geometry around at least one of our RCB stars. Looking at the visibility curves (Figs 2, 5 and 7), asymmetric structure is apparent in RY Sgr, may also exist in V CrA and is possible for V854 Cen but is not constrained at present (see Section 3). Our geometrical models provide a PA of the asymmetric distribution of dust (or cluster) and by observing these objects over time, we can learn whether there is a preferential dust ejection axis or plane. Although the geometrical models only give the simplistic version of one large 'cluster', this represents an overall asymmetry found in the production of dust.

Only RY Sgr has more than one epoch of data and asymmetries are detected in both 2005 and 2007. The RY Sgr 2005 model has an asymmetry placed at a PA of 79° and in 2007 the PA of the asymmetry was at 175°, approximately 90° from the 2005 epoch. It is important to note that although the geometrical model, comprised of a star, a Gaussian shell and a cluster, gives us the lowest reduced χ^2 value, the same PAs are also found if an elliptical uniform disc is used implying that there is indeed some sort of asymmetry in this direction. However, the determination of whether there is an overall preferential plane will have to wait until a time series of observations that measure the location of several 'clusters' over time are obtained .

According to the DUSTY models, RY Sgr, V CrA and V854 Cen all have dust shells with approximately the same $R_{\rm DUSTY}$ despite other differences. This distance may be a common characteristic between RCB stars or it may be a bias of the simplistic DUSTY approach to modelling these complex stars. An insight into this question will require more data and investigation.

5.4 Large-scale dust distribution and composition

MIDI spectra were obtained subsequently to the interferometric data. These spectra correspond to the flux from the central 250 mas of the sources. In addition to the MIDI spectra, *ISO*/SWS spectra exist for RY Sgr and V854 Cen and *Spitzer*/IRS data exist for V CrA and V854 Cen. *ISO*/SWS records flux through a slit with an aperture of 14×20 arcsec^2 (Sloan et al. 2003) and *Spitzer*/IRS SL spectra were taken through a 3 arcsec wide slit with a very long length (Houck et al. 2004). By comparing these spectra, we can determine where the majority of the flux is coming from. For RY Sgr, the 2007 MIDI spectra are $\sim$20 per cent fainter than the 1997 *ISO*/SWS spectra (the RY Sgr MIDI 2005 and 2007 data were identical within 5 per cent, so only the 2007 data are used in this paper). For V CrA, the 2007 MIDI spectra are $\sim$30 per cent brighter than the 2005 *Spitzer*/IRS spectra. These changes are within the expected error bars for the respective instruments (e.g. MIDI spectra can change by 10–15 per cent within a few minutes depending on fluctuations in the atmosphere; Chesneau 2007). In addition, the flux from the stars will have varied by an unknown amount between the *ISO*, *Spitzer* and MIDI epochs. Taking this into consideration, we determine that the majority of the flux is coming from the inner 250 mas of the source for both RY Sgr and V CrA. On the other hand, for

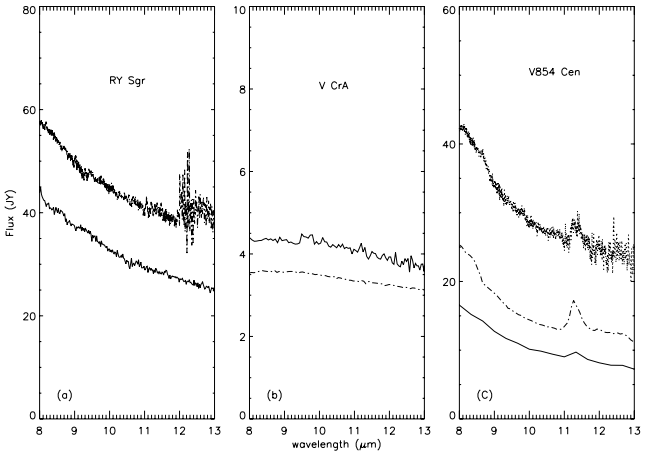

Figure 10. (a) Spectra of RY Sgr: MIDI – lower curve, *ISO* – upper curve. (b) Spectra of V CrA: *Spitzer* – lower curve, MIDI – upper curve. (c) Spectra of V854 Cen: MIDI – lower curve, *Spitzer* – middle curve, *ISO* – upper curve.

V854 Cen the 2008 *Spitzer*/IRS spectra are ∼55 per cent brighter than the 2007 MIDI spectra and the 1996 *ISO*/SWS spectra are ∼165 per cent brighter than the 2007 MIDI spectra. These higher percentages cannot be accounted for by uncertainties or normal variability. This implies that there is a significant amount of circumstellar material outside of the region observed with MIDI, possibly in another outer shell. V854 Cen is known to have a 5 arcsec circumstellar nebula at UV and mid-IR wavelengths (Clayton & Ayres 2001; Lagadec, private communication). The comparisons of all spectra obtained for the RCB stars are shown in Fig. 10.

Generally RCB stars, including R CrB and RY Sgr, show no features in the mid-IR (Lambert et al. 2001; Kraemer et al. 2005). The exception is V854 Cen which shows polycyclic aromatic hydrocarbons (PAH)-like emission features (Lambert et al. 2001; García-Hernández et al. 2010). Our MIDI spectra for RY Sgr and V CrA appear to be featureless, but the spectrum of V854 Cen show emission features from ∼8 μm and at ∼11.5 μm. These features may be due to hydrogenated amorphous carbon (HAC), C_{60}, or PAHs (Clayton et al. 1995; García-Hernández et al. 2010; Evans et al., in preparation). RCB stars are known to have variable emission features, and C_{60} may be present only for a short time after the initial decline when carbon gas is condensing into dust (Whitney, Balm & Clayton 1993; Goeres & Sedlmayr 1992). These emission features have an impact on V854 Cen's visibility curves (Fig. 7) which exhibit a drop at the features' wavelengths. The dust responsible for the features is over-resolved, i.e. more extended. In other words, dust associated with the emission feature is blocking light from the central unresolved source and the total visibility is lower than the model at 8 μm by 21 per cent. This drop is proportional to the amount of extra flux that the feature contributes to the SED (23 per cent) at 8 μm. A smaller drop in visibility and excess in the SED are also noted at 11.5 μm.

Our observations with the VLTI have shed light on both the large- and small-scale structure and composition of RCB stars. The large extended shell and emission features found for V854 Cen are atypical for RCB stars and need to be investigated further. In addition, RY Sgr's visibility curves, in both 2005 and 2007, may reveal a slight drop at 8–9 μm, but is not as evident as the drop for V854 Cen. This hints at the ability of high angular resolution observations to detect chemical structure that cannot be revealed by spectrometry.

5.5 Dust grain size

Standard MRN dust distribution (Mathis et al. 1977) uses $a_{\rm min} = 0.005$ μm and $a_{\rm max} = 0.1$ μm for graphite. However, in our models, larger grains of $a_{\rm max} = 2$ μm are needed in order to accurately fit both the SED and the visibility curves. Tests were also performed to see how only large grains ($a_{\rm min} = 0.2$ μm and $a_{\rm max} = 2.0$ μm) would affect the DUSTY fitting. Using $a_{\rm min} = 0.005$ μm and $a_{\rm max} = 2$ μm provided the best results. While we could achieve adequate fits using only large grains ($a_{\rm min} = 0.2$ μm and $a_{\rm max} = 2$ μm), the slopes of the visibility curves could not be matched as accurately for RY Sgr and V854 Cen without smaller grains. Without the smaller grains, the screening effect (discussed in Section 3.2) cannot occur. Additionally, using only larger grains caused $R_{\rm inner}$ to decrease by a factor of 2 due to the efficiency of heat absorption. Such a strong dependence of $R_{\rm inner}$ on the dust grain size leaves this parameter poorly constrained. It is unclear what the larger dust grains mean in physical terms. It is unlikely that the dust grains are actually this large. DUSTY may be requiring large dust grains because there is a heavy level of asymmetry which it cannot account for. More tests need to be done to test all the effects that the changing grain size has on DUSTY fits of RCB stars.

5.6 Future observations

MIDI's spatial resolution is about 10 mas. This resolution is not sufficient to accurately detect and measure the dust-forming regions of RCB stars. However, the Astronomical Multiple BEam combineR (AMBER), a VLTI instrument which observes in the near-IR, has a spatial resolution of 1–2 mas (Wittkowski 2007). This resolution would be enough to directly measure the inner regions of the circumstellar envelope and track the change in the location of individual dust clumps. To do so, frequent observations are needed (at least a monthly cadence) using the same set of baselines and PAs to guarantee that the same dust cluster or clump is tracked. Although such an observational campaign would require a significant telescope time allocation, the return would be justified: RCB stars are among a few classes of merged objects. In addition, it is likely that the short RCB phase may guarantee that the merger has just taken place. Studying a merger aftermath environment will lead to tremendous insight into the physics of the merger, with possible insight into Type Ia supernova detonation and gravitational wave physics.

ACKNOWLEDGMENTS

We acknowledge with thanks the variable star observations from the AAVSO International Database contributed by observers worldwide and used in this research. The research leading to these results received funding from the European Community's Seventh Framework Programme under Grant Agreement 226604 and from a Macquarie University Research Excellence Scholarship (SNB). We also wish to thank the anonymous referee for valuable comments and suggestions.

REFERENCES

Alcock C. et al., 2001, ApJ, 554, 298
Asplund M., Gustafsson B., Kameswara Rao N., Lambert D. L., 1998, A&A, 332, 651
Asplund M., Gustafsson B., Lambert D. L., Rao N. K., 2000, A&A, 353, 287
Cardelli J. A., Clayton G. C., Mathis J. S., 1989, ApJ, 345, 245

Chesneau O., 2007, New Astron. Rev., 51, 666
Clayton G. C., 1996, PASP, 108, 225
Clayton G. C., Ayres T. R., 2001, ApJ, 560, 986
Clayton G. C., Whitney B. A., Stanford S. A., Drilling J. S., 1992, ApJ, 397, 652
Clayton G. C., Kelly D. M., Lacy J. H., Little-Marenin I. R., Feldman P. A., Bernath P. F., 1995, AJ, 109, 2096
Clayton G. C., Bjorkman K. S., Nordsieck K. H., Zellner N. E. B., Schulte-Ladbeck R. E., 1997, ApJ, 476, 870
Clayton G. C., Kerber F., Gordon K. D., Lawson W. A., Wolff M. J., Pollacco D. L., Furlan E., 1999, ApJ, 517, L143
Clayton G. C., Geballe T. R., Bianchi L., 2003, ApJ, 595, 412
Clayton G. C., Herwig F., Geballe T. R., Asplund M., Tenenbaum E. D., Engelbracht C. W., Gordon K. D., 2005, ApJ, 623, L141
Clayton G. C., Geballe T. R., Herwig F., Fryer C., Asplund M., 2007, ApJ, 662, 1220
Crause L. A., Lawson W. A., Henden A. A., 2007, MNRAS, 375, 301
de Laverny P., Mékarnia D., 2004, A&A, 428, L13
Deroo P., van Winckel H., Verhoelst T., Min M., Reyniers M., Waters L. B. F. M., 2007, A&A, 467, 1093
Ercolano B., Barlow M. J., Storey P. J., 2005, MNRAS, 362, 1038
Feast M. W., 1986, in Hunger K., Schoenberner D., Kameswara Rao N., eds, Proc. IAU Colloq. 87, Hydrogen Deficient Stars and Related Objects. Reidel, Dordrecht, p. 151
Feast M. W., Carter B. S., Roberts G., Marang F., Catchpole R. M., 1997, MNRAS, 285, 317
Fujimoto M. Y., 1977, PASJ, 29, 331
Furlan E. et al., 2006, ApJS, 165, 568
García-Hernández D. A., Lambert D. L., Kameswara Rao N., Hinkle K. H., Eriksson K., 2010, ApJ, 714, 144
Geballe T. R., Evans A., Smalley B., Tyne V. H., Eyres S. P. S., 2002, Ap&SS, 279, 39
Gillett F. C., Backman D. E., Beichman C., Neugebauer G., 1986, ApJ, 310, 842
Goeres A., Sedlmayr E., 1992, A&A, 265, 216
Hanner M., 1988, in NASA Conf. Publ. 3004, Infrared Observations of Comets Halley and Wilson and Properties of the Grains. NASA, Washington, DC, p. 22
Houck J. R. et al., 2004, ApJS, 154, 18
Iben I., Jr, Tutukov A. V., Yungelson L. R., 1996, ApJ, 456, 750
Ivezic Z., Elitzur M., 1997, MNRAS, 287, 799
Ivezic Z., Nenkova M., Elitzur M., 1999, User Manual for DUSTY. Univ. Kentucky Internal Report, http://www.pa.uky.edu/∼moshe/dusty
Kraemer K. E., Sloan G. C., Wood P. R., Price S. D., Egan M. P., 2005, ApJ, 631, L147
Lambert D. L., Rao N. K., Pandey G., Ivans I. I., 2001, ApJ, 555, 925
Lawson W. A., Cottrell P. L., 1997, MNRAS, 285, 266
Lawson W. A., Cottrell P. L., Kilmartin P. M., Gilmore A. C., 1990, MNRAS, 247, 91
Lawson W. A. et al., 1999, AJ, 117, 3007
Leão I. C., de Laverny P., Chesneau O., Mékarnia D., de Medeiros J. R., 2007, A&A, 466, L1
Leinert C. et al., 2003, Ap&SS, 286, 73
Mathis J. S., Rumpl W., Nordsieck K. H., 1977, ApJ, 217, 425
Ohnaka K. et al., 2003, A&A, 408, 553
Ohnaka K., Izumiura H., Leinert C., Driebe T., Weigelt G., Wittkowski M., 2008, A&A, 490, 173
Pojmanski G., 2002, Acta Astron., 52, 397
Pugach A. F., 1977, Inf. Bull. Variable Stars, 1277, 1
Ratzka T., Leinert C., Henning T., Bouwman J., Dullemond C. P., Jaffe W., 2007, A&A, 471, 173
Ratzka T. et al., 2009, A&A, 502, 623
Renzini A., 1979, in Westerlund B. E., eds, Astrophysics and Space Science Library Vol. 75, Stars and Star Systems, Mass Loss and Stellar Evolution. Reidel, Dordrecht, p. 155
Saio H., Jeffery C. S., 2002, MNRAS, 333, 121
Sloan G. C., Kraemer K. E., Price S. D., Shipman R. F., 2003, ApJS, 147, 379
Tisserand P. et al., 2009, A&A, 501, 985
Walker H. J., 1985, A&A, 152, 58
Walker H. J., 1986, in Hunger K., Schoenberner D., Kameswara Rao N., eds, Proc. IAU Colloq. Vol. 87: Hydrogen Deficient Stars and Related Objects. Reidel, Dordrecht, p. 407
Webbink R. F., 1984, ApJ, 277, 355
Whitney B. A., Balm S. P., Clayton G. C., 1993, in Sasselov D. D., ed., ASP Conf. Ser. Vol. 45, Luminous High-Latitude Stars, Dust Formation in R-Coronae Stars. Astron. Soc. Pac., San Francisco, p. 115
Wittkowski M., 2007, New Astron. Rev., 51, 639
Woitke P., Goeres A., Sedlmayr E., 1996, A&A, 313, 217

This paper has been typeset from a TEX/LATEX file prepared by the author.